JOURNAL OF MATERIALS SCIENCE **40** (2005) 4753–4759

The dependence of mechanical properties on structure in low alloy steel forgings

S. MAROPOULOS*,†, N. RIDLEY
Materials Science Centre, The University of Manchester, Grosvenor Street, Manchester M1 7HS, UK
E-mail: maropou@otenet.gr

Published online: 08 July 2005

The mechanical properties of two heat-treated steel forgings, manufactured from medium carbon Ni-Cr-Mo-V steels have been measured and compared. Microstructural characteristics such as martensite packet and lath size, dislocation density and precipitate size and distribution were measured and used in a detailed quantitative analysis of the relation between microstructural characteristics and proof stress. It was found that the microstructural differences identified could well account for the differences in tensile strength between the materials. Electron microcopy indicated that temper embrittlement leading to intergranular fracture may be responsible for the differences in transition temperature.

1. Introduction

There are several factors that contribute to the high strength of martensite [1–4]. These include (a) carbon in solid solution, (b) the high dislocation density of lath martensite, (c) precipitation of carbides in tempered martensite structures, (d) restriction of the dislocation free path by twin boundaries in plate martensite, and (e) substitutional solid solution strengthening.

Assuming that the effects of the individual strengthening mechanisms are additive, several Hall-Petch type equations have been developed which take into account the various strengthening mechanisms that contribute to the yield strength of tempered martensite structures [1, 3, 5, 6].

A general equation of the form

$$\sigma_y = \sigma_i + \sigma_{ss} + \sigma_p + \sigma_d + \sigma_{sg} + \sigma_t + K_y d^{-1/2} \quad (1)$$

emerges, where σ_y is the yield strength, σ_i is the friction stress, mainly the Peierls stress, σ_{ss} is the solid solution strengthening, σ_p is the precipitate strengthening, σ_d is the dislocation strengthening, σ_{sg} is the strengthening due to subgrains, σ_t is a crystallographic texture strengthening parameter, K_y is the yield stress intensity factor, and d is the grain diameter.

The present work attempts to evaluate the individual strengthening contributions of the tempered martensite in two electroslag refined (ESR) low alloy steel forgings. The two steels investigated, J and H, were of similar compositions and had almost identical heat treatment, yet their mechanical properties were quite different. The work reported here was aimed at understanding the reasons for the differences in tensile strength and transition temperature between the two steels, and between the two ends of the forging made from steel H.

2. Experimental

Sections from two good quality electroslag remelted cylindrical steel forgings were supplied. These included three slices from both ends and the middle part of a forging made of steel J and three slices from each end of a forging made of steel H. The end of the forging that originated from the top and from the bottom part of the H-steel ingot will, subsequently, be referred to as steel M and steel B, respectively. The chemical compositions of the three materials are listed in Table I.

Heat treatment of the materials was as follows. For J-steel (i) austenitise at 890°C for 4 h and air cool, (ii) austenitise at 870°C for 5 h and oil quench, (iii) temper at 630°C for 6 h and oil quench, (iv) stress-relieve at 400°C for 4 h and air cool. For H-steel (i) austenitise at 880°C for 4 h and air cool (ii) austenitise at 870°C for 5 h and oil quench, (iii) temper at 640°C for 8 h and air cool. The H-steel forging, however, failed to meet the designer's specifications for Brinell hardness and was re-austenitised at 870°C for 5 h and oil quenched, and tempered at 620°C for 8 h. On testing, it failed at both ends for the proof stress and at the M end for the impact strength. It was then re-tempered at 625°C for 8 h and air cooled but still failed at the M end for the impact strength.

*Author to whom all correspondence should be addressed.
†*Present Address*: Pl. 25 Martiou 5, 50100 Kozani, Greece.

0022–2461
DOI: 10.1007/s10853-005-0780-y

TABLE I Chemical analysis by Quantivac, wt%

Steel	C	Ni	Cr	Mo	V	Cu	Mn	Si	P	S
J	0.35	3.26	0.88	0.66	0.22	0.23	0.52	0.18	0.006	0.005
M	0.29	3.10	0.77	0.57	0.14	0.25	0.52	0.15	0.006	0.006
B	0.29	3.09	0.80	0.57	0.16	0.25	0.53	0.12	0.002	0.004

Duplicate tensile tests were performed using size 14 Hounsfield specimens at a cross-head speed of 0.5 mm min^{-1}. Impact testing was carried out in the temperature range 25 to –196°C. In order to find the 50% fracture appearance ductile-to-brittle transition temperatures ($50\%FATT$), the amounts of cleavage and ductile fracture on the fracture surfaces were measured, using a low power microscope ($\times 10$). Both tensile and Charpy specimens were machined parallel to the longitudinal direction of the forging.

For fractographic studies, specimens were examined with a Philips SEM 505 electron microscope fitted with an X-ray detector. Martenste packet sizes were obtained from measurements of the quasicleavage facet size which has been shown to be equivalent to the packet size [7, 8]. Facet sizes were obtained by averaging the dimensions of at least 150 facets on broken Charpy specimens as observed using the SEM.

Transmission electron microscopy of thin foils and extraction replicas was carried out with a Philips 301 electron microscope. Carbide sizes were measured from micrographs of extraction replicas taken at appropriate magnifications. The mean free carbide path, P, and the interparticle spacing, λ, were calculated from the following equations [9]:

$$P = \frac{4}{3} r \frac{(1 - V_f)}{V_f}, \tag{2}$$

$$\lambda = \sqrt{\frac{\pi r P}{2(1 - V_f)}} - \frac{\pi r}{2}, \tag{3}$$

where r is the average particle radius and V_f the theoretical volume fraction of carbides. The value of V_f was calculated, assuming that all the carbon was out of solution at the tempering temperatures used and in the form of Fe_3C, although solubility product calculations showed that a small amount of carbon was in the form of V_4C_3.

In order to overcome problems with accurate measurement of the local foil thickness, which can lead to large errors in the dislocation density values, dislocation densities were determined using X-ray diffraction line broadening with an analysis by Williamson and Smallman [10]. They derived the following equation for deducing the dislocation density from the cell (or particle) size, t

$$\rho(m\,m^{-3}) = 3n/t^2 \tag{4}$$

where t is in metres.

The analysis assumes that the material has a block (cell) structure with the dislocations lying in the boundaries between the blocks. The factor n is the number of dislocations per block face. Taking $n = 1$, as in the present work, gives a minimum dislocation density and could apply to annealed or very severely deformed metals. This is a justified assumption in the present work, where it was observed that the dislocations were usually arranged into fine cells within the martensite laths [8]. The cell size t is associated with coherently diffracting domains of the lattice such as grains or cells.

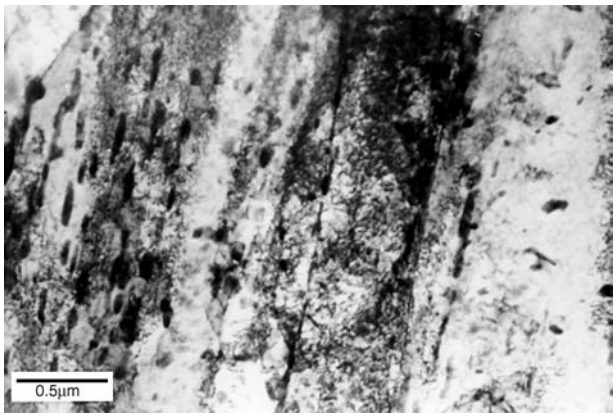

Figure 1 The microstructure of the steels in the as-received condition showing retainment of lath morphology, steel J.

3. Results and discussion

3.1. Microstructures

The microstructure of the steels in the as-received condition is shown in Fig. 1. The lath morphology of quenched martensite was preserved at the high tempering temperatures used. The laths contained dislocations arranged in sub-grains and a high density of carbide particles, Fig. 2. The lath widths were similar in all three steels and varied from approximately 0.2 to 0.5 μm. Other observations, made by electron microscopy, showed the existence of areas where the martensite lath boundaries are not well defined and lath free regions mainly in steels M and B, Fig. 3. It is believed that they arise from areas in the martensitic structure where tempering has resulted in the disappearance of lath boundaries due to a lower carbide density in these regions [8, 11–13]. The results of structural measurements are given in Table II.

3.2. Mechanical tests

Important tensile and Charpy data are summarised in Table III. As can be seen there is a surprising difference in mechanical properties between the steels in view of their similar compositions and thermal history. Steel J exhibits higher tensile strength, higher hardness as well as better fracture toughness properties, when compared to steel H. In addition there is a difference between the two ends of the H steel forging with the M part being slightly stronger and harder, but of considerably lower fracture toughness, than end B. No difference in mechanical properties along the length of the steel J forging was observed.

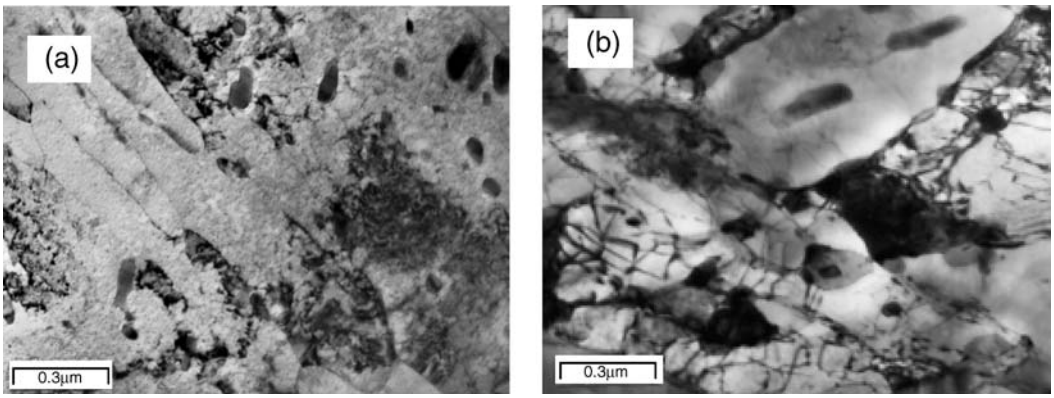

Figure 2 (a) Ill-defined lath boundaries, (b) dislocation sub-cells and carbide particles, steel *M*.

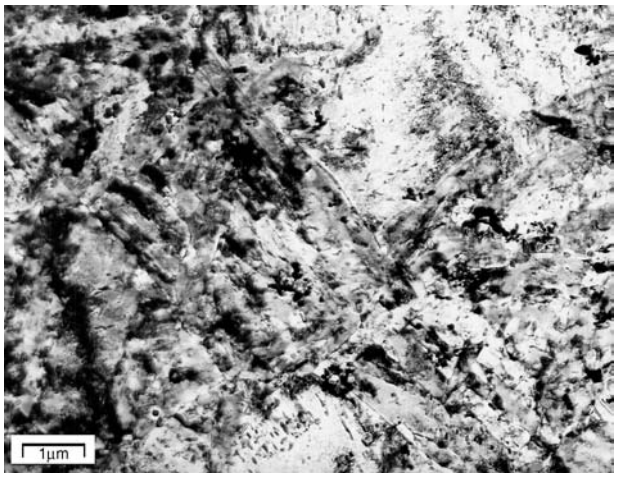

Figure 3 Lath free regions in steel *B*.

3.3. Contributions to 0.2% proof stress

(a) *Peierls stress*, σ_i. The Peierls stress is that required to move a dislocation through an otherwise perfect lattice. The simplest estimate of this stress [1, 14] is based on a sinusoidal force relationship and predicts a value of $10^{-4}G$, where G is the shear modulus. Experimental estimates [1, 15] of σ_i in iron at ambient temperature are in the range 13–55 MNm^{-2}. Smith and Hehemann [1] and Speich and Swann [15] for a steel of similar composition (4340 steel) used a value of 41 MNm^{-2} and the same will be adopted here.

(b) *Solid solution strengthening.* The solid solution strengthening term includes both the interstitial strengthening from carbon in solution, σ_{is} and the substitutional strengthening from the other alloying elements present, σ_{ss}. The cementite in the three steels appears to be fully precipitated and therefore the matrix carbon content must be close to the equilibrium value of ~0.01% in all three steels. This will contribute approximately 137 MNm^{-2} to the proof stress [16]. Lacy and Gensamer [17] considered the effects of various substitutional elements on the yield strength of bcc iron. Assuming that the effects of the individual elements are additive the contribution from substitutional solution strengthening can be determined, Table IV.

(c) *Work hardening.* The work hardening that occurs in attaining the 0.2% proof stress also contributes to the strength [1]. The stress-strain curves obtained for the three steels show that they strain harden only slightly between the elastic limit and 0.002 strain. Therefore the work hardening contribution, σ_{wh}, will be small, Table IV.

TABLE II Carbide characteristics, martensite lath size and dislocation density

Steel	$\%V_f$	r (μm)	P (μm)	λ (μm)	R_{calc} (μm)	Lath size (μm)	Disl.density $(m\ m)^{-3}$
J	5.08	0.044	1.096	0.213	0.216	0.336	1.5×10^{14}
M	4.46	0.050	1.442	0.266	0.260	0.404	1.12×10^{14}
B	4.46	0.041	1.185	0.219	0.238	0.370	1.12×10^{14}

TABLE III Mechanical properties (P.S. = proof stress, E = elongation, R.A. = reduction of area, H_V = Vicker's hardness, n = work hardening coefficient, FATT = fracture appearance transition temperature, USE = upper shelf energy)

Steel	0.2% P.S. (MPa)	$\%E$	%R. A.	H_V	n	50% FATT (°C)	USE (J)
J	1068	16	50	361	0.047	−84	79
M	875	18	52	321	0.060	−10	94
B	864	21	64	312	0.065	−22	125

TABLE IV Contributions to total strength from various sources, MPa

Steel	σ_c	σ_{wh}	σ_{ss}	σ_{ps}	σ_{ls}	σ_p	σ_d ($=\sigma_A$)	σ_B	σ_L	σ_{rms}	$\sigma_{observed}$
J	178	10	332	127	265	173	221	1085	1306	1107	1068
M	178	15	321	100	90	141	191	845	1036	866	875
B	178	18	303	107	78	166	191	850	1041	871	864

σ_c = Peierls stress, σ_i (41 MPa) + interstitial strengthening ,σ_{is}(136 MPa).
σ_{wh} =work hardening contribution.
σ_{ss} = substitutional strengthening.
σ_{ps} = packet size contribution, $\sigma_{ps}(\text{MPa}) = 9d^{-1/2}$, d = packet size in mm ,Equation 6.
σ_{lb} = lath boundary strengthening, σ_{lb} (MPa) = $8.62 \times 10^{-2} w^{-1}$, w= lath width in mm, Equation 7.
σ_p = precipitation hardening, σ_p (MPa) = $(6.26/\lambda)\ln(D/2.48 \times 10^{-4})$, D = mean planar intercept diameter of a precipitate (μm) and λ = surface to surface precipitate spacing (μm), Equation 9.
$\sigma_d(=\sigma_A)$ = dislocation strengthening,$\sigma_d = 2\alpha Gb\rho^{l/2}$, where α = 0, 88, $G(= 8.3 \times 10^4$ MPa) is the shear modulus for pure iron, $b(=$ 0.248 nm) is the Burgers vector, ρ is the dislocation density, Equation 5.
$\sigma_B = \sigma_i + \sigma_{is} + \sigma_{ss} + \sigma_{lb} + \sigma_{ps} + \sigma_p$, Equation 11.
$\sigma_L = \sigma_A + \sigma_B$, linear summation.
$\sigma_{rms} = (\sigma_A^2 + \sigma_B^2)^{1/2}$

(e) *Dislocation strengthening.* Smith and Hehemann [1] considered a constant dislocation strengthening contribution during tempering. However, several studies [3, 5, 16] showed that the dislocation density and therefore the strengthening resulting from dislocation interactions changes considerably during tempering.

The following relationship by Taylor [18] was used to calculate the dislocation density contribution to the strength

$$\sigma_d = 2\alpha G b \rho^{l/2} \tag{5}$$

where $G(= 8.3 \times 10^4$ MNm$^{-2})$ is the shear modulus for pure iron and $\mathbf{b}(= 0.248$ nm) is the Burgers vector, ρ is the dislocation density, and α is a constant. A range of α values is available in the literature [19]. A value of 0.88 determined by Roberts *et al.* [20] was adopted in the present work. A number of other workers have also shown a preference for this value [3, 19, 20]. The calculated values of σ_d are given in Table IV.

(f) *Grain boundary strengthening.* There is much argument in the literature on which microstructural feature should be taken as the effective grain size as the strength of lath martensite has been related to the packet size and to the lath size [1, 2, 4]. In the present work, both types of boundary are assumed to produce strengthening, in accord with previous suggestions [3, 7, 21].

Martensite packet size is an important microstrctural parameter in determining the strength of as-quenched dislocated martensite [3, 21]. A strong Hall-Petch type dependence of the yield strength on martensite packet size was found by a number of investigators [2, 3, 22] in as quenched martensite. However, Swarr and Krauss [22] observed that in tempered martensite the strong dependency of strength on packet size was significantly reduced and indeed the 0.6% proof stress Hall-Petch plot was a horizontal line. The steep slope of the Hall-Petch plot for as-quenched martensite was attributed to carbon segregation to packet and lath boundaries. Tempering reduced K_y because, although the packet size was unaltered, the distribution of carbon at the boundaries changed from segregation on an atomic scale to concentration in the form of fine carbides at the packet and lath boundaries.

If a regression analysis is applied to the experimental results of Swarr and Krauss [22], the following equation for the packet size contribution is obtained

$$\sigma_{ps}(\text{MPa}) = 9d^{-1/2} \tag{6}$$

The values of σ_{ps}, calculated from Equation 6 are given in Table IV.

In their model for the yield strength of tempered martensite, Smith and Hehemann [1] used the average lath width as the grain size and found good agreement with experimental results. They suggested, however, that the strength was related to the reciprocal width of the laths rather than the reciprocal square root of this width, as required by the Hall-Petch equation, and developed the following equation for the lath boundary contribution

$$\sigma_{lb}(\text{MPa}) = 8.62 \times 10^{-2} w^{-1} \tag{7}$$

where w is the lath width in millimetres.

In the present study, all steels contained considerable amounts of lath free regions (Table V). The "equivalent" size, calculated from the relationship

$$l = A_f l_1 + (1 - A_f) 1_2 \tag{8}$$

where A_f is the area fraction of the lath free regions, 1_1 is the approximate width of the lath free regions and 1_2 the 1ath width, was considered, therefore, the appropriate parameter for Equation 6.

(g) *Precipitation hardening.* A frequently used [23–25] version of the Orowan equation by Hírsch and Humphreys [25] can be expressed as

$$\sigma_p(\text{MNm}^{-2}) \frac{6.26}{\lambda} \ln \frac{D}{2.48 \times 10^{-4}} \tag{9}$$

where D is the mean planar intercept diameter of a precipitate and λ is the surface to surface precipitate spacing, λ and D are in micrometres.

In the present work, the above equation was employed to predict the strengthening contribution from the precipitates using the data in Table II. The values calculated are given in Table IV.

TABLE V Area fraction and approximate size of lath free regions

Steel	A_f(%)	Size (μm)
J	12	1.5
M	24	4.5
B	27	5

3.4. Predicted vs measured 0.2% proof stress

The contributions to the total strength (0.2% proof stress) from the various sources are given in Table IV. Although the summation of the components of strength has usually been linear, the rms (root mean square) summation

$$\sigma_{rms} = \left(\sigma_A^2 + \sigma_B^2\right)^{1/2} \tag{10}$$

has been considered by a number of workers as more appropriate [19, 26]. Kocks and co-workers [27] have identified σ_A and σ_B as strengthening associated with two distinct types of obstacle which can be broadly defined as forest dislocations ($\sigma_d = \sigma_A$) and particles, respectively [26]. In addition, they considered it appropriate to include in the particle strengthening term σ_B all the other components of the yield stress, and a similar procedure is adopted in the present work. Thus σ_A is the dislocation strengthening, σ_d, due to interactions between forest dislocations and mobile dislocations,

which lead to strain hardening, and σ_B is given by

$$\sigma_B = \sigma_i + \sigma_{is} + \sigma_{ss} + \sigma_{lb} + \sigma_{ps} + \sigma_p \qquad (11)$$

The results of both a linear and an rms summation are given in Table IV. The linear addition of the strength components σ_L gives a gross overestimate when compared with the observed values of the proof stress, with the errors ranging from +18 to +22%. The rms summation σ_{rms}, however, results in values that are in good agreement with the experimental results, with the errors ranging from –1.8 to +3.6%. A number of other workers [3, 5, 28] have also found that the rms addition was a better description of their structures. The above results are not, however, considered to be absolute proof that the rms summation is more suitable for predicting the strength, since significant errors in σ_L may be caused by overestimates of the individual strengthening components.

The present analysis makes several assumptions and uses previously derived data for α, K_y, the Peierls stress, σ_i, and the interstitial strengthening, σ_{is}, component. The term σ_d is calculated from indirect measurements of dislocation densities. In determining the precipitation hardening component, the stoichiometric volume fraction was used and complete precipitation of carbon as cementite and vanadium carbide was assumed. However, the terms σ_p and σ_d would not be expected to be responsible for the large errors.

It is thought that, if the linear summation is more suitable, the overestimates arise from the interstitial strengthening term (137 MNm^{-2}) and/or the lath boundary component. The former was estimated by Cox [16] and was used by Smith and Hehemann [1] but does not appear in the analyses of other workers. Smith and Hehemann [1] attributed grain boundary strengthening to the lath boundaries of their tempered microstructures and found good agreement with experimental results. However, the lath boundaries in the present work were not always well defined, Fig. 2, and there were often lath free regions observed, Fig. 3, and it may be that they did not contribute to the strength. Subtracting the lath boundary component yields values much closer to the measured proof strengths, with errors in the range –2.5 to +11%.

3.5. Transition temperature

A linear relationship between transition temperature of martensitic steels and the inverse root of the grain size has been observed by a number of workers [2, 3, 14, 15]. A study on the effect of varying austenitising temperatures on the properties of *J* steel [3] showed that the transition temperature could be described by the relationship

$$50\%\ FATT(^\circ\mathrm{C}) = -31 + 0.16(\sigma_d + \sigma_p) - 9.5\, d^{-1/2} \qquad (12)$$

where σ_d and σ_p are the dislocation and precipitation components of the yield strength, respectively, and d is the cleavage size.

Applying the above equation to the materials studied here gave 50% *FATT* values of –102, –84 and –88°C steels *J*, *M* and *B*, respectively. As can be seen there is fairly good agreement between predicted and observed values for *J* steel. However, for steels *M* and *B* there is a marked difference in the two values suggesting that there must be other factors also contributing to the observed differences in *FATT*.

Another factor affecting the ductile-brittle transition temperature is temper embrittlement leading to intergranular fracture. One would not expect temper embrittlement to occur in the steels examined here in view of their low phosphorus contents, the presence of molybdenum and the heat treatment applied. However, it was observed that the grain boundaries in steels *M* and *B* etch much darker than in steel *J* (Fig. 4).

In the past, preferential etching of prior austenite grain boundaries by aqueous picric acid was regarded as an indication of temper emrbittlement [29].

The fracture surfaces of specimens broken at –196°C were nickel-plated and sectioned through the fractures. The fracture sections were examined grain by grain with the SEM to estimate the relative amounts of cleavage and of intergranular fracture. No intergranular fracture was observed in steel *J*. However, steels *M* and *B* showed 5.4 and 4.3% intergranular fracture, respectively (Fig. 5).

Therefore, there must be a small contribution to the observed differences in *FATT* from the intergranular fracture that occurs in steels *M* and *B*. Further it is suggested that impurity intergranular segregation caused

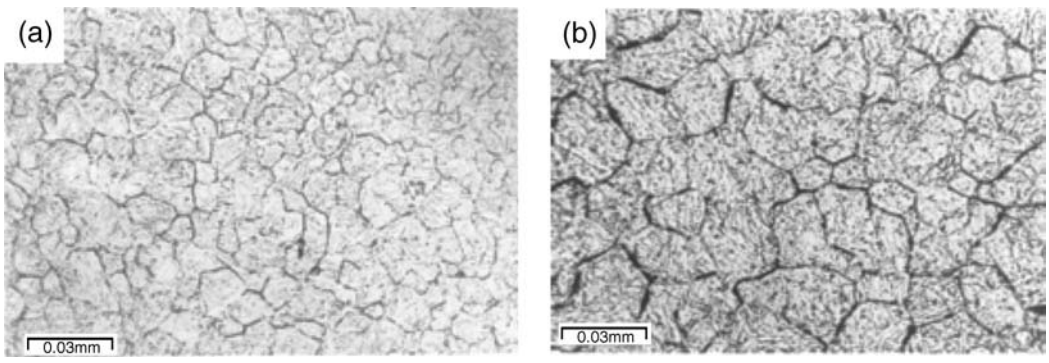

Figure 4 The prior austenite grain structure (a) steel *J*, (b) steel *M*.

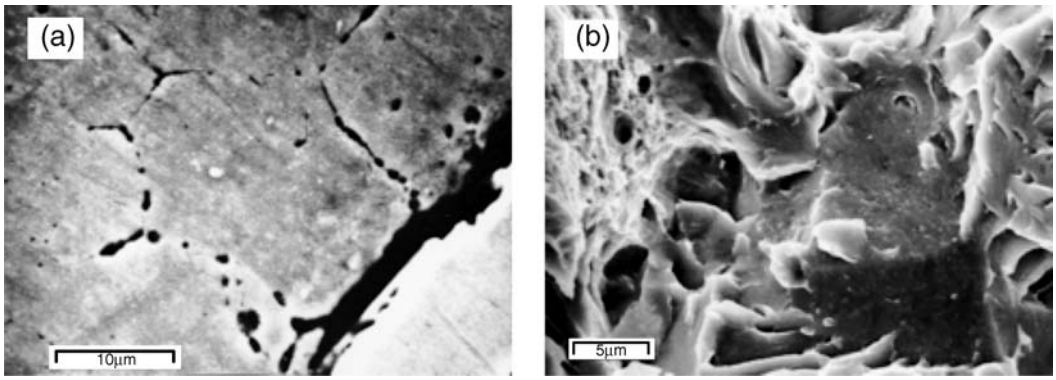

Figure 5 Intergranular fracture in steel *M* (a) Ni-plated fracture surface, (b) SEM.

by temper embrittlement could account for more of the observed differences in *FATT* than is deduced from the amount of intergranular fracture measured.

It is believed that in steels *M* and *B* small amounts of impurities segregate on prior austenite grain boundaries and thus result in weakening of the boundaries which, however, are still stronger than the slip planes [30]. This weakening of grain boundaries means that they will no longer act as strong barriers in the crack propagation process, so that the cleavage stress is lowered and therefore the transition temperature is raised. In some cases, where there are sufficient amounts of impurities on grain boundaries to reduce the pre-existing grain boundary surface energy sufficiently, intergranular fracture occurs.

Previous studies on steels similar to the ones examined here report that an increase in susceptibility to intergranular fracture coincides with the precipitation of M_3C carbides on grain boundaries [31–34]. Long time tempering is known to result in precipitation of molybdenum-rich carbides, M_6C and/or $(FeMo)_3C$, thus lowering the amount of molybdenum in solution that can be effective in inhibiting temper embrittlement [33]. It is believed that there are two reasons for the intergranular fracture observed in steels *M* and *B*.

Firstly the carbides in steels *M* and *B* were richer in molybdenum than in steel *J*, presumably due to the double tempering they received. Table VI lists the average molybdenum contents of twenty analyses on carbide particles in the three steels. The amounts of molybdenum left in solution, calculated from the relative volume fractions of Fe_3C, are also given in Table VI. It can be seen that in steels *M* and *B* the amount of molybdenum in solution is too low to completely prevent the occurrence of temper embrittlement by phosphorus.

A second reason is thought to be the air cooling used after tempering for the *H*-steel forging (*M* and *B*) as opposed to oil quenching used for steel *J*. Cooling rate is known to be a major factor in determining structure and properties in HSLA steels [31, 32, 35]. The cooling rate during air cooling of the thick section *H*-steel forging is not particularly fast, and it may be that there is sufficient time for the impurities to segregate on prior austenite grain boundaries while the steel is in the temper embrittling temperature region.

The use of Auger spectroscopy, which could give direct evidence for any phosphorus segregation on prior austenite grain boundaries, was considered impractical in this case where only a small percentage of the grains fracture intergranularly.

To examine whether the air cooling used after tempering for steels *M* and *B* was in any way responsible for their higher transition temperatures compared to steel *J*, the following set of experiments were carried out. Charpy blanks of steels *M* and *B* were tempered at 600°C for 1/2 h and oil quenched and tested at –40°C. No improvement was however observed in the impact energy. The results of Powers [36] indicate that with steels containing molybdenum, high tempering temperatures and long tempering times are required for de-embrittlement. A second set of Charpy blanks were, therefore, tempered at 620°C for 1 h and oil quenched. On testing at –40°C a considerable improvement in impact energy, by 56 and 94% for steel *M* and *B* respectively, was observed while the Vickers hardness was little affected.

To examine whether air cooling after tempering wou1d have any effect on the impact energy in steel *J*, Charpy blanks were tempered at 610°C for 1/2 h. and air cooled and tested at –40°C. The results showed no difference in impact energy with that of the as-received material. It is, therefore, concluded that a small amount of temper embrittlement, resulting in intergranular fracture, occurs in steels *M* and *B* due to the air cooling of the *H*-steel forging, which allows sufficient time for some impurity segregation to occur on prior austenite grain boundaries.

TABLE VI Amount of molybdenum (wt.%) in solution in Fe_3C and in the matrix

Steel	Mo in the matrix	Mo in Fe_3C
J	0.39	5.6
M	0.17	8.4
B	0.16	8.6

4. Conclusions

The higher tensile strength of steel *J* can be attributed to several factors. Firstly, the slight differences in substitutional element content (silicon, chromium, molybdenum and nickel) can account for part of the observed differences in strength. In addition, the increased

dislocation density of steel *J*, together with its higher volume fraction of finer, more closely spaced, cementite and vanadium carbide particles are also believed to contribute to its higher strength. Finally, the finer grain structure of steel *J*, that is smaller martensite packet and lath size, may also be responsible for its increased tensile strength.

The 0.2% proof stress values predicted using a rms summation of the strengthening contributions are in good agreement with experimentally measured values whereas a linear summation leads to an overestimate probably due to the lath boundary strengthening term.

Intergranular fracture caused by temper embrittlement is believed to contribute to the higher *FATT* of steels *M* amd *B*. This is caused by two factors. Firstly the precipitation of Mo rich carbides depletes the amount of Mo in solution available to inhibit temper embrittlement. Secondly impurity segregation to prior austenite grain boundaries results from the lower cooling rate of the air-cooling employed after tempering.

Acknowledgements

The present work was carried out with support from the Defence Research Agency (DRA) formerly the Procurement Executive, Ministry of Defence (U.K.).

References

1. D. W. SMITH and R. F. HEHEMANN, *J. Iron. Steel. Inst.* **209** (1971) 476.
2. L. A. NORSTROM and O. VINGSBO, *Met. Sci.* **12** (1979) 677.
3. S. MAROPOULOS, J. D. H. PAUL and N. RIDLEY, *Mater. Sci. Tech.* **9** (1993) 1014.
4. Q. LI, *ibid. A* **361** (2003) 385.
5. L. MALIK and J. A. LUND, *Met. Trans.* **3A** (1972) 1403.
6. C. H. YOUNG and H. K. D. H. BHADESHIA, *Mater. Sci. Technol.* **10** (1994) 209.
7. T. GLADMAN and F. B. PICKERING, in "Yield, Flow and Fracture of Polycrystals," edited by T. N. Baker (Applied Science, London, 1983) p. 141.
8. S. MAROPOULOS, N. RIDLEY and S. KARAGIANNIS, *Mater. Sci. Eng. A* **380** (2004) 79.
9. R. N. CARON and G. KRAUSS, *Met. Trans.* **3** (1972) 2381.
10. G. K. WILLIAMSON and R. E. SMALLMAN, *Philos. Mag.* **1** (1956) 34.
11. B. D. CRAIG and G. KRAUSS, *Met. Trans.* **11A** (1980) 1799.
12. W. J. NAM, C. S. LEE and D. Y. BAN, *Mater. Sci. Eng. A* **289** (2000) 8.
13. D. H. SHIN, Y. S. KIM and E. J. LAVERNIA, *Acta Mater.* **49** (2001) 2387.
14. F. R. NABARRO, *Proc. Phys. Soc.* **59** (1947) 256.
15. G. R. SPEICH and P. R. SWANN, *J. Iron. Steel. Inst.* **203** (1956) 480.
16. A. R. COX, *Trans. Japan. Inst. Met.* **9** (1968) 118.
17. C. E. LACY and M. GENSAMER, *Trans. Amer. Soc. Met.* **32** (1944) 88.
18. G. I. TAYLOR, *Proc. R. Soc. A* **145** (1934) 362.
19. T. N BAKER, in "Yield, Flow and Fracture of Polycrystals," edited by T. N. Baker (Applied Science, London, 1983) p. 235.
20. W. ROBERTS, S. KARLSSON and Y. BERGSTROM, *Mater. Sci. Eng.* **11** (1973) 247.
21. Y. TOMITA and K. OKABAYASHI, *Met. Trans.* **17A** (1986) 1203.
22. T. SWARR and G. KRAUSS, *ibid.* **17A** (1976) 41.
23. L. M. BROWN and R. K. HAM, in "Strengthening Methods in Crystals," edited by A. Kelly and R. B. Nicholson (Elsevier, London, 1971) p. 9.
24. M. C. CHATURVEDI, D. J. LLOYD and D. W. CHUNG, *Met. Sci.* **10** (1976) 373.
25. P. B. HIRSCH and F. J. HUMPHREYS, in "Physics of Strength and Plasticity," edited by A. S. Argon, (MIT Press, Cambridge, USA, 1969) p. 189.
26. J. IRVINE and T. N. BAKER, *Mater. Sci. Eng.* **64** (1984) 123.
27. U. F. KCOCKS, A. S. ARGON and M. F. ASHBY, *Prog. Mat. Sci.* **19** (1975) 156.
28. M. E. KASSNER, A. K. MILLER and O. D. SHERBY, *Met. Trans.* **13A** (1982) 1977.
29. J. M. CAPUS, *J. Iron. Steel. Inst.* **200** (1962) 922.
30. D. F. STEIN, W. C. JOHNSON and C. L. WHITE, in "Grain Boundary Structure and Properties," edited by G. A. Chadwick and D. W. Smith (Academic Press, London, 1976) p. 301.
31. H. ITOH, *J. Japanese Soc. Mater. Sci.* **51** (2002) 418.
32. *Idem.*, *ibid.* **51** (2002) 549.
33. K. W. ANDREWS, H. HUGHES and D. J. DYSON, *Jour. Ir. St. Inst.* **210** (1972) 337.
34. E. D. HONDROS and D. MCLEAN, in "Grain Boundary Structure and Properties," edited by G. A. Chadwick and D. W. Smith, (Academic Press, London, 1976) p. 353.
35. S. DAS, A. GHOSH, S. CHATTERJEE and P. RAMACHANDRA RAO, *Scripta Mater.* **48** (2003) 51.
36. A. E. POWERS, *J. Iron Steel Inst.* **186** (1957) 513.

Received 25 November 2004
and accepted 2 March 2005